SFN #336 31-38

藤井　通子

今日の一覧

- Growing and Trapping Pebbles with Fragile Collisions of Particles in Protoplanetary Disks
  - Paola Pinilla, Christian T. Lenz, Sebastian M. Stammler
- Observational constraints on the likelihood of 26Al in planet-forming environments
  - Megan Reiter
- Kinematic Analysis of a Protostellar Multiple System: Measuring the Protostar Masses and Assessing Gravitational Instability in the Disks of L1448 IRS3B and L1448 IRS3A
  - Nickalas K. Reynolds et al.
- Accretion and outflow activity in proto-brown dwarfs
  - B. Riaz, J. Bally
- Survey of ortho-H2D+ in high-mass star-forming regions
  - G. Sabatini et al.
- The TW Hya Rosetta Stone Project II: Spatially resolved emission of formaldehyde hints at low-temperature gas-phase formation
  - Jeroen Terwisscha van Scheltinga et al.
- The SEDIGISM survey: first data release and overview of the Galactic structure
  - SEDIGISM Collaboration
- From parallel to perpendicular – On the orientation of magnetic fields in molecular clouds
  - D. Seifried et al.

From parallel to perpendicular – On the orientation of magnetic fields in molecular clouds

MNRAS

D. Seifried, S.Walch, M.Weis, S. Reissl, J. D. Soler, R. S. Klessen, P. R. Joshi

- シミュレーションから、ダストのpolarization mapを作って、3次元の密度や２次元のcolumn densityと磁場の向きの関係を調べた
  - 観測との比較がモチベーション
- 初期の磁場が5μGあたりを境に、10^2-10^3 cm^{-3}くらいの高密度領域で磁場が並行から垂直に変わる（flipが起こる）
  - 3-5μGは銀河系の平均的な値に近い
- しかし、2次元で見ると（Projected Rayleigh Statisticsという手法を使う）、10^{21}-$10^{21.5}$ cm^{-2} あたりでflipが起こるはずだが、投影しているせいで、いつもそうなるとは限らない
  - これが、観測で見えている多様性の要因かも。

- シミュレーション２種類
  - Colliding Flow (CF): 128 pc x 32 pc x 32 pc, collision vel. 13.6 km/s
  - SILCC-Zoom: 500 pc x 500 pc x 5 kpc section of galactic disk, 3 μ G
    - SN injection (15 SNe /Myr)
- AMR code: FLASH 4.3 磁気流体計算
- Radiative transfer: POLARIS

In order to test the relative orientation of the magnetic field direction and density structures, we take $\theta = 2\,\phi$, where ϕ is the relative orientation angle between the plane-of-sky projected magnetic field $\mathbf{B}_{\rm POS}$, inferred from the polarization direction by rotating it by 90°, and the tangent to the column density (N) isocontour (Soler et al. 2017). This is equivalent to the angle between the observed polarization direction $\mathbf{E}$ and the gradient of the column density, ∇N, which allows us to calculate the angle as

$$\phi = \arctan\left(|\nabla N \times \mathbf{E}|, \nabla N \cdot \mathbf{E}\right) . \quad (8)$$

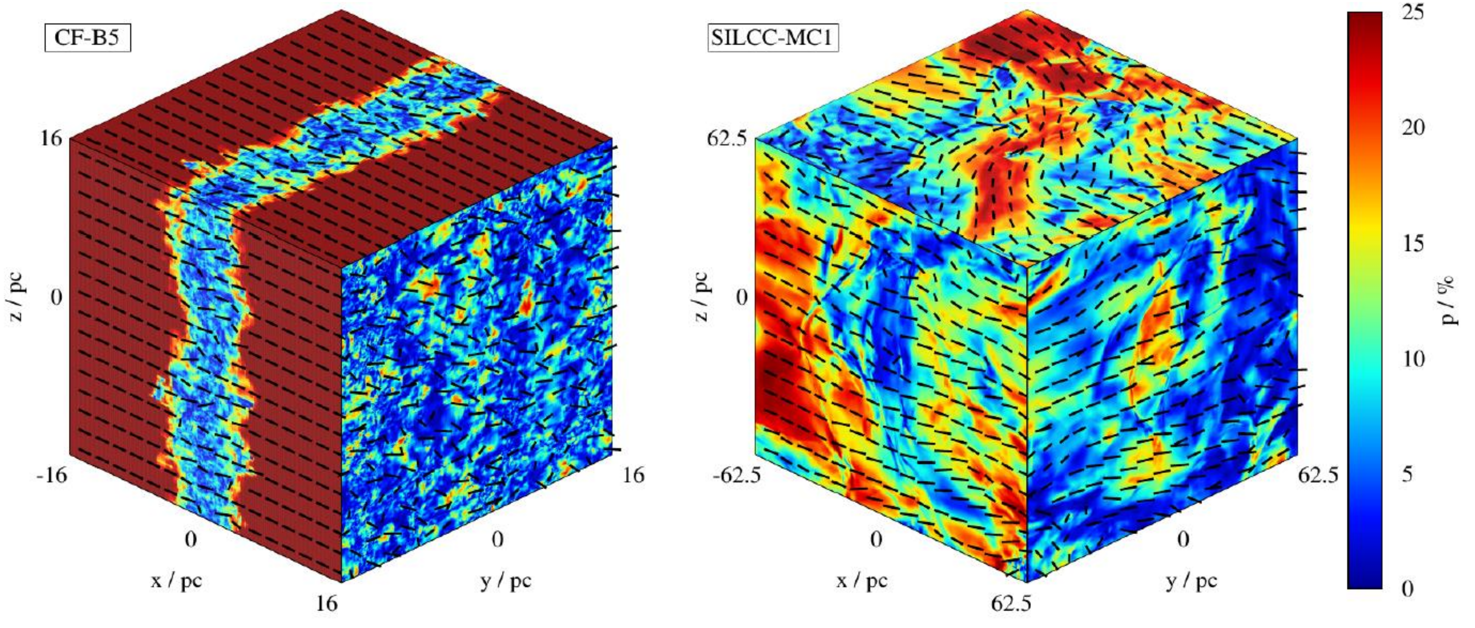

Figure 2. Synthetic polarization maps obtained with POLARIS of run CF-B5 (left) and SILCC-MC1 (right) at $t_{\rm evol} = 3$ Myr. The figure shows the polarization degree from 3 orthogonal directions (colour coded) and the polarization direction rotated by 90° (black bars) to

- Projected Rayleigh Statistic, Z

CF

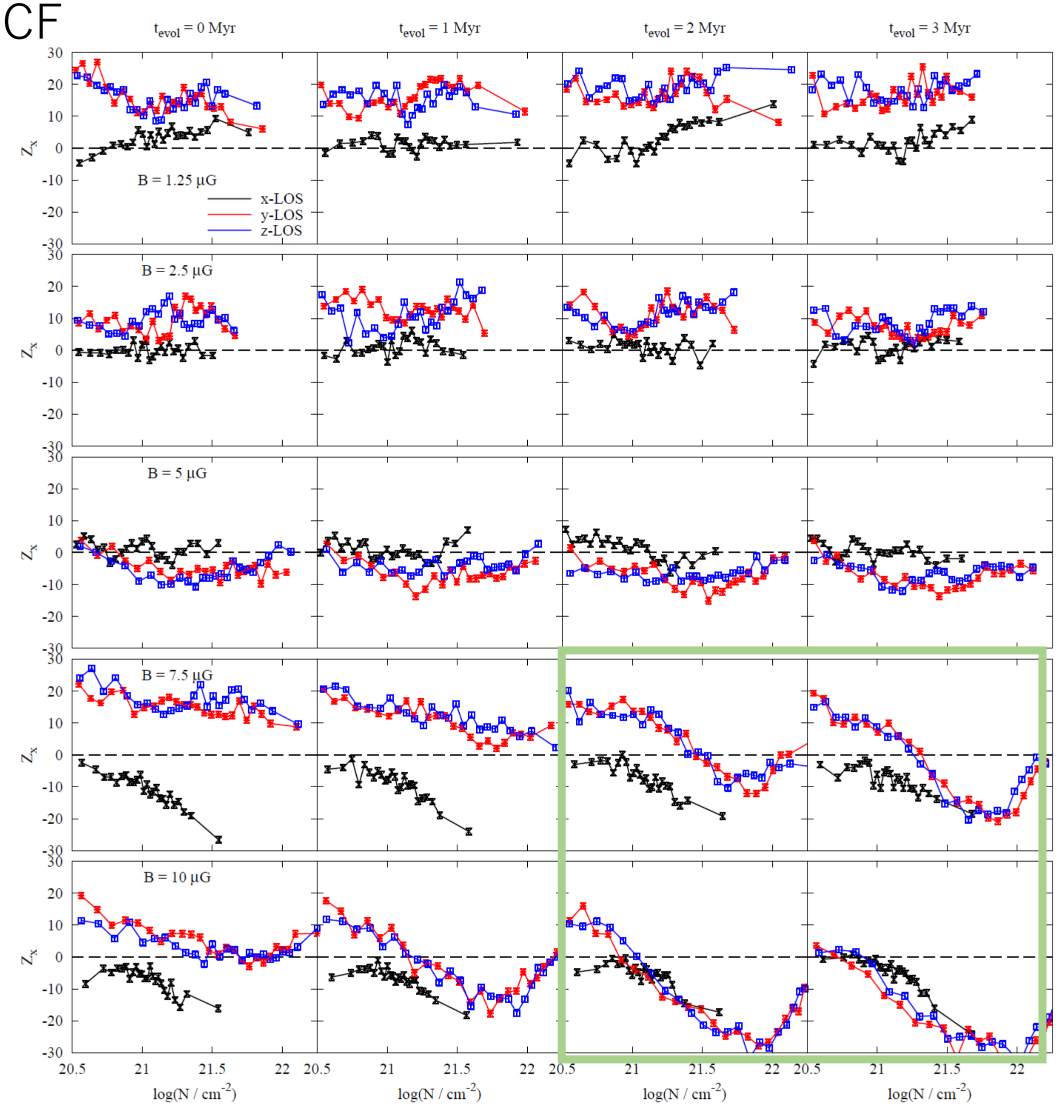

Figure 3. Time evolution (from left to right) of the PRS, Z_x, of the CF runs with increasing magnetic field strength (from top to bottom) for three different LOS. A preferentially perpendicular orientation ($Z_x < 0$) at high column densities is only present for runs with field strength $\geq$ 5 μG. In addition, for these runs the perpendicular orientation becomes more pronounced at later times. For the weak field runs, the magnetic field remains mostly parallel to the density structures or shows no preferred direction. The uncertainty σ_{Z_x} of each bin (shown by horizontal bars) is rather minor.

平行

垂直

SILCC-Zoom　全部初期3μG

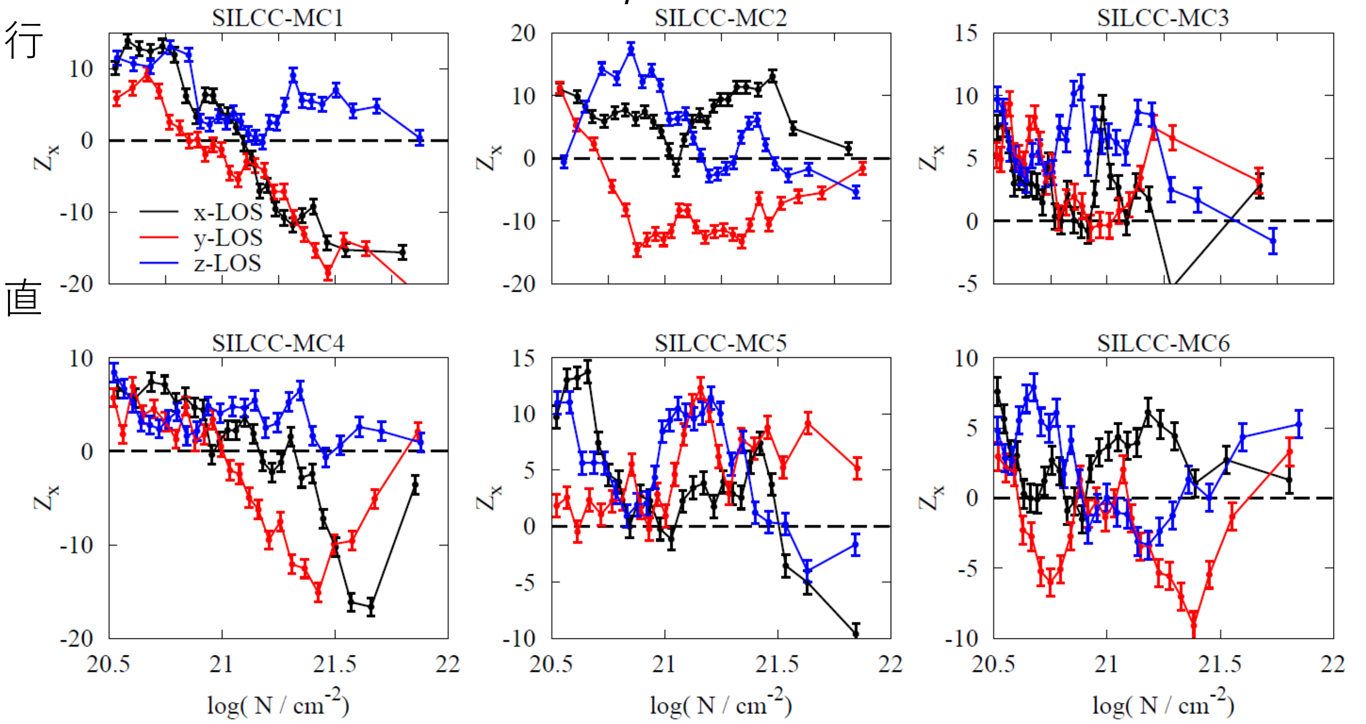

Figure 7. PRS, Z_x, of the six SILCC-Zoom simulations at t_{evol} = 3 Myr for three different LOS. Overall, there is a large variety of shapes in agreement with the moderate field strength of 3 μG. On average, there appears to be a slight trend of decreasing Z_x with increasing N. Note the different ordinate scalings.

複数のサンプルについて、磁場の揃い具合
（Projected Rayleigh Statistic）

$$Z_x = \frac{\Sigma_i^{n_{\rm ind}} \cos\theta_i}{\sqrt{n_{\rm ind}/2}}$$

The TW Hya Rosetta Stone Project II: Spatially resolved emission of formaldehyde hints at low-temperature gas-phase formation

Terwisscha van Scheltinga et al.

- H_2CO のオルソ-パラ比（OPR）のTW Hyaでの分布を調べた
- 60auより内側ではOPRは3、60au以遠では徐々に下がり2.0pm0.5
- 外側のspin temperatureは12Kで、rotational temperature 30-40 Kより低い
  - Gas-phase formation: “warm”な状況だとOPR=3くらい。
  - Solid-state formation: coldだと、OPR＜3
- 円盤の外側でOPR＜3だが、solid-stateではなくgas-phaseで H_2COの形成が起こっていそう
  - Emission profileがなめらかなので同じメカニズムが働いていそう
  - OPRは外側へ行くにつれて減少
  - 外側では、低温で、低いOPRになるようなgas-phase formationが起こっているのでは？

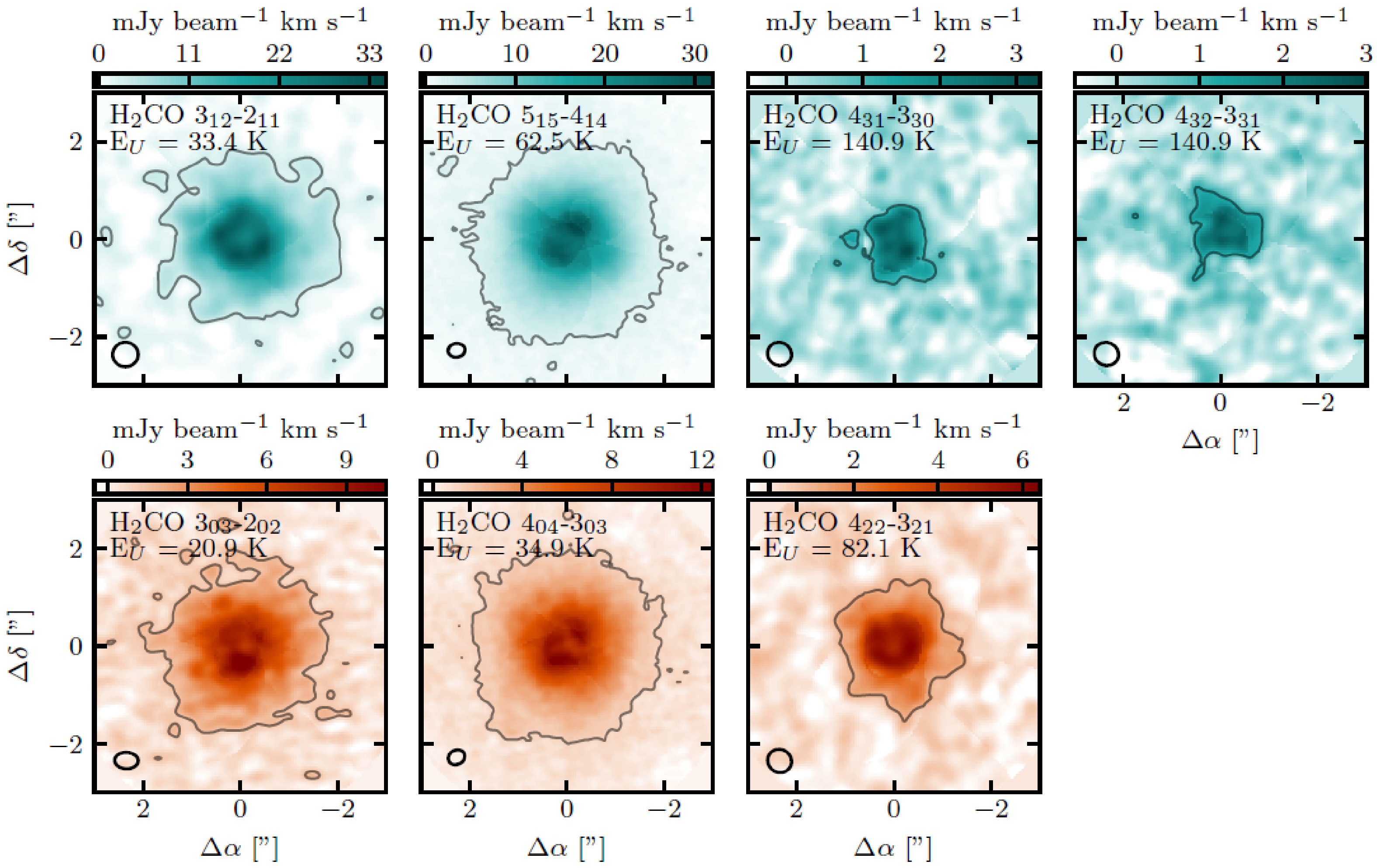

Figure 3. Keplerian masked velocity integrated emission of observed H_2CO transitions at native spatial resolution (V_{LSR} = 1.83–3.83 km s^{-1}). Top row: ortho-spin isomer transitions; bottom row: para-spin isomer transitions. The contour in each panel depicts 3σ, where σ for each transition is taken from Table 2. Beam sizes are indicated by the ellipse in the left-bottom corner of each panel.

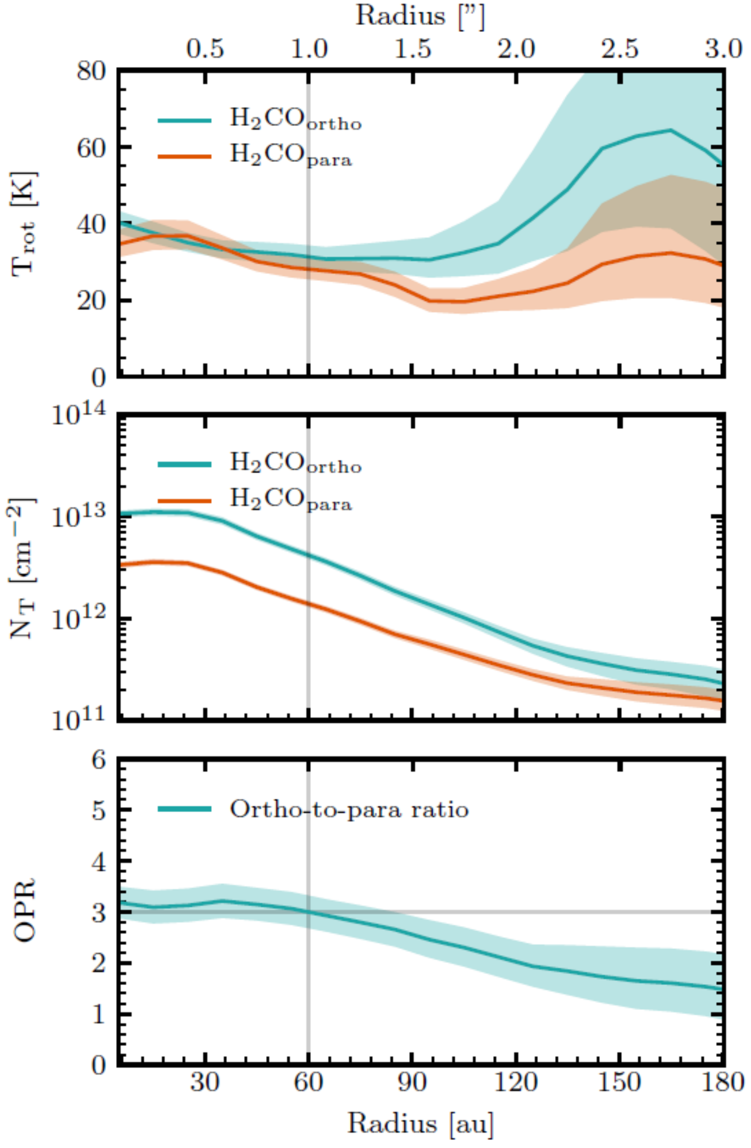

Figure 6. Radially resolved H_2CO temperature (top panel), column densities (middle panel), and OPR (bottom panel) of H_2CO obtained from our rotational diagram analysis using the radial emission profiles of Fig. 4. Teal and bronze colors represent the ortho- and para-spin isomers, respectively. Shaded areas depict 1σ uncertainties. The gray vertical and horizontal line depict the mm-dust continuum edge and the high temperature OPR limit of 3.0, respectively.